INTENSE FOCAL AND REYNOLDS STRESS STRUCTURES OF A SELF-SIMILAR ADVERSE PRESSURE GRADIENT TURBULENT BOUNDARY LAYER

Atsushi Sekimoto, Vassili Kitsios, Callum Atkinson
Laboratory for Turbulence Research in Aerospace and Combustion,
Department of Mechanical and Aerospace Engineering, Monash University, Clayton 3800, AUSTRALIA
atsushi.sekimoto@monash.edu.au

Javier Jiménez
School of Aeronautics, Universidad Politécnica de Madrid, 28040 Madrid, Spain

Julio Soria
Laboratory for Turbulence Research in Aerospace and Combustion,
Department of Mechanical and Aerospace Engineering, Monash University, Clayton 3800, AUSTRALIA
Department of Aeronautical Engineering, King Abdulaziz University
Jeddah 21589, KINGDOM OF SAUDI ARABIA

Abstract

The turbulence statistics and structures of a self-similar adverse pressure gradient turbulent boundary layer (APG-TBL) are investigated using direct numerical simulation (DNS) of the flow at the verge of separation. The desired self-similar APG-TBL is achieved by a modification of the far-field velocity boundary condition. The required wall-normal velocity in the far-field to produce the necessary adverse pressure gradient was estimated based on the analytical free-stream streamwise velocity distribution for a flow at the point of separation, and the assumption that the streamlines of the outer flow follow the growth of the boundary layer thickness. The APG-TBL develops over a momentum thickness based Reynolds number upto 12000, and achieves a self-similar region of constant friction coefficient, pressure velocity and shape factor. Turbulence statistics in this region show self-similar collapse by using the scaling of the external velocity and the displacement thickness. In this study, the structure of the APG-TBL is investigated using topological methodology and visualisation techniques for a zero pressure gradient turbulent boundary layer (ZPG-TBL) and for the self-similar APG-TBL. The second invariants of the velocity gradient tensor (VGT), which are representative of coherent structures dominated by vortical motions, show a stark difference in the structure and location of coherent vortical structures that exists between the self-similar APG-TBL and a ZPG-TBL. Further details based on the structure and distributions of the invariants of VGT and intense Reynolds stress structures of the self-similar APG-TBL are presented.

Introduction

The turbulent boundary layer (TBL) subjected to strong adverse pressure gradient (APG) is frequently found to be challenging as it pertains to flow separation prediction, development of appropriate turbulence models for the efficient design and flow control. Many aspects of turbulent structures in APG-TBL flows and the scaling of turbulence statistics remain unresolved. As wall-bounded flows approach separation, the classical inner wall scaling using the friction velocity, u_τ, is not applicable and the flows with strong APG resemble free-shear flows. Some attempts for determining the appropriate length and velocity scale in strong APG-TBLs have been reported in comparison with free shear flows (Gungor *et al.*, 2016). However, the conditions of the upstream flow also contaminates experimental measurements and statistics profile obtained by simulations, so that the appropriate scaling remains an open question.

Here, we focus on canonical self-similar APG-TBL, in the sense that each of the terms in the governing equations have the same proportionality with streamwise position (Townsend, 1976, 1960; Mellor & Gibson, 1966; Castillo & Wang, 2004). An achievement of a self-similar APG-TBL minimises the effect of upstream flow and history (Kitsios *et al.*, 2015, 2016), and detailed information on the large-scale motions and the distribution of small-scale vortices would shed light on the characteristics of simple APG-TBLs.

In this paper, the structure of TBLs is investigated using topological methodology and visualisation techniques (Chong *et al.* (1998); Soria & Cantwell (1994); Soria *et al.* (1994)) for a zero pressure gradient turbulent boundary layer (ZPG-TBL) and for the self-similar APG-TBL. The second invariants of the velocity gradient tensor (VGT), which is representative of coherent structures dominated by vortical motions, shows a stark difference in the structure and location of coherent vortical structures that exists between the self-similar APG-TBL and a ZPG-TBL. Further details based on the structure and distributions of

the invariants of VGT and intense Reynolds stress structures (Lozano-Durán *et al.*, 2012; Lozano-Durán & Jiménez, 2014; Soria *et al.*, 2016; Dong *et al.*, 2017) of the self-similar APG-TBL and how these compare to the ZPG-TBL are also presented.

Numerical Methodology

The boundary layer is simulated in a three-dimensional rectangular domain over a no-slip smooth wall. The axes in the streamwise, wall-normal and spanwise directions are x, y and z. The corresponding velocity fluctuation with respect to the time-averaged mean (U, V, W) are (u, v, w). The spanwise boundary condition is periodic, and the Fourier expansion with $2/3$ dealiasing is applied. The compact finite differences in staggered grids are used in x and y (Lele, 1992). The direct numerical simulation (DNS) is performed by the code of Borrel *et al.* (2013). We use modified version of the recycling method introduced by Sillero *et al.* (2013), and the desired self-similar APG-TBL is achieved by a modification of the far-field velocity boundary condition. The required wall-normal velocity in the far-field to produce the necessary adverse pressure gradient was estimated based on the analytical free-stream streamwise velocity distribution for a flow at the point of separation (Mellor & Gibson, 1966)

$$U_e(x) \propto x^m \quad \text{with } m = -0.23, \tag{1}$$

and the assumption that the streamlines of the outer flow follow the growth of the boundary layer thickness.

The reference velocity,

$$U_e(x) \equiv U_\Omega(x, y_{\max}), \quad U_\Omega(x,y) \equiv -\int_0^y \Omega_z(x,y')\mathrm{d}y' \tag{2}$$

where Ω_z is the mean spanwise vorticity and $y_{\max}$ is the wall-normal position of maximum U_Ω. The displacement and momentum thickness are defined using spanwise vorticity Lighthill (1963) as:

$$\delta_1(x) = \frac{-1}{U_e}\int_0^{y_{\max}} y\Omega_z(x,y)\mathrm{d}y, \tag{3}$$

$$\delta_2(x) = \frac{-2}{U_e^2}\int_0^{y_{\max}} yU_\Omega\Omega_z(x,y)\mathrm{d}y - \delta_1(x). \tag{4}$$

The Reynolds number is $Re_{\delta 1} \equiv U_e\delta_1/\nu$, where ν is the kinetic viscosity.

The domain of interest (DoI) of the strong APG-TBL is chosen as the region where the shape factor is $H \approx 2.35$. Hereafter, x_{DoI} denotes the beginning of DoI, where $Re_{\delta 1}(x_{\mathrm{DoI}}) = 4800$ for ZPG- and a mild APG-TBL ($\beta = 1$, Kitsios *et al.* (2016)), and $Re_{\delta 1}(x_{\mathrm{DoI}}) = 22200$ for a strong APG-TBL ($\beta = 39$, Kitsios *et al.* (2017)). β is the nondimensional pressure gradient by Clauser (1954).

Results

Self-similar statistics

By using above reference velocity and outer scale, U_e and δ_1, the turbulence statistics of the strong APG-TBL collapses within the domain of interest as shown by Kitsios *et al.* (2017). Figure 1(a–c) show the averaged velocity fluctuations and the tangential Reynolds stress $\tau_{xy} \equiv -\langle uv\rangle$, and the data of mild APG-TBL, ZPG-TBL and a channel database at $Re_\tau \approx 4200$ (Lozano-Durán & Jiménez, 2014), whose displacement thickness is $\delta_1 = 0.094h$ from eq. (3), are also compared. It is indicated that velocity fluctuations in a strong APG-TBL, which does not have logarithmic region, are mainly produced in the outer layer.

The driving mechanism of strong APG-TBL is the local shear as in the wall-bounded turbulence (Jiménez, 2013). Figure 1(d) shows the Corrsin shear parameter (Corrsin, 1958), $S_c \equiv (\partial U/\partial y)q^2/\varepsilon$, where $q^2 \equiv u^2 + v^2 + w^2$ and ε is the dissipation rate, as a function of $y/\delta_1(x)$, in comparison with the other wall-bounded turbulence. The typical value in the outer region is $S_c \approx 7$–10 both in homogeneous shear turbulence (HST) (Sekimoto *et al.* (2016)) and in the logarithmic layer of wall-bounded flows (Jiménez, 2013). The near-wall peak of APG-TBL decreases as the layer grows (not shown), and the weaker local mean shear close to the wall would not generate intense turbulence structures. On the other hand, in the outer region $y/\delta_1 \approx 1$, S_c is roughly constant value ($S_c \approx 9$) in good agreements with both HST, turbulent mixing layers (Wygnanski & Fiedler, 1970) and at the top of the logarithmic layer in wall-bounded turbulence.

Topological analysis and flow visualisation

The topological methodology is applied at each $y/\delta_1 \approx 0.1$ 0.3 and 1.0 of a strong APG-TBL and ZPG-TBL ($y^+ \approx 20$, 60 and 300 for ZPG-TBL). The self-similar scaling of the small-scale property, $\omega' \equiv \sqrt{\omega_i\omega_i}$, in the turbulent outer region is estimated from the approximate energy balance of kinetic energy and self-similar scaling, $\nu\omega'^2 \approx -\tau_{xy}S \approx U_e^3/\delta_1$, where ν is the kinematic viscosity, and τ_{xy} is the tangential Reynolds stress and $S = \partial U/\partial y$ is the mean shear. Then the invariants are estimated as $Q \sim Re_{\delta_1}U_e^2/\delta_1^2$ and $R \sim Re_{\delta_1}^{3/2}U_e^3/\delta_1^3$

The figure 4 shows the joint probability density function of the second and third invariant of the velocity gradient tensor, which clearly indicates that the dissipative fine-scale vortices are generated at $y/\delta_1 \approx 1$ in APG-TBL, at which the peaks of the velocity fluctuations are observed. On the other hand, the near-wall mean shear generates strong vortical structures for ZPG-TBL.

The instantaneous three-dimensional geometry of the self-similar APG is visualised in figure 4. The isosurfaces of intense Reynolds stress seem to be separated from the wall and that is true for the fine-scale vortex clusters represented by isosurfaces of the second invariant of the velocity gradient tensor. Most of events are generated in the outer region of APG-TBL, and the interaction of the local shear and the Reynolds stress (uv-structures) are of great interest, in comparison with those in a mild APG or zero-pressure-gradient (ZPG) TBL, turbulent mixing layer and homogeneous shear turbulence (HST).

Intense Reynolds stress

As shown in figure 4(a), the intense Reynolds stress structures (uv-structures) are detached from the wall and that is true for the fine-scale vortex clusters represented by isosurfaces of the second invariant of the velocity gradient tensor (as shown in figure 4(b)).

Ejections (Q2) and sweeps (Q4) are identified by $\tau_{xy}^* < -C_\tau u^* v^*$, where $\tau_{xy}^* = \langle uv\rangle/(U_e(x)^2)$, $u^* = u/U_e(x)$, $v^* =$

$v/U_e(x)$ and C_τ is a constant threshold. As shown in figure 4(a,c), the volume fraction and the scaled stress conditioned on the *uv*-structure indicate that ejections and sweeps are balanced at a symmetric point, $y/\delta_1 \approx 0.88$, for a strong APG-TBL ($\beta = 39$), and at $y/\delta_1 \approx 1.35$ for a mild APG-TBL ($\beta = 1$), independently of C_τ. Here we define such distance from the wall as δ_s, which corresponds to the location of an inflection point of the mean velocity profile in the outer layer. Ejections mainly interact with the free stream at around $y/\delta_s \gtrsim 2$, and on the other hand, sweeps have larger contributions on the Reynolds stress than ejections below the symmetric points, $y/\delta_s < 1$. The wall effect is limited within $y/\delta_s \lesssim 0.5$ for both mild and strong APG-TBL. The mild APG-TBL has another balanced point near the wall, at which the near-wall peaks of velocity fluctuations and the energy production are observed, and on the other hand, the strong APG-TBL at the verge of separation does not represent such a near-wall effect and it behaves like more or less a free shear flow.

At the end, contributions of intense Reynolds stress structures on the statistics are shown in figure 4(b,d). These percolation analysis of Q2s and Q4s indicate that, as increasing C_τ, strong large-scale structures are organised at around a inflection point in the outer region, producing outer-layer peaks of velocity fluctuations. These results are consistent with those obtained in the experiments (Krogstad & Skåre, 1995; Schatzman & Thomas, 2017). Further investigations on the intense Reynolds stress structures in the self-similar APG-TB are on-going.

ACKNOWLEDGEMENTS

The authors acknowledge the research funding from the Australian Research Council and European Research Council, and the computational resources provided by NCI and the Pawsey Supercomputer Centre both supported by the Australian government and PRACE supported by the EU.

REFERENCES

Borrel, G., Sillero, J. A. & Jiménez, J. 2013 A code for direct numerical simulation of turbulent boundary layers at high Reynolds numbers in BG/P supercomputers. *Comp. Fluids* **80**, 37–43.

Castillo, Luciano & Wang, Xia 2004 Similarity analysis for nonequilibrium turbulent boundary layers. *J. fluids Eng.* **126** (5), 827–834.

Chong, MS, Soria, J, Perry, AE, Chacin, J, Cantwell, BJ & Na, Y 1998 Turbulence structures of wall-bounded shear flows found using DNS data. *J. Fluid Mech.* **357**, 225–247.

Clauser, Francis H 1954 Turbulent boundary layers in adverse pressure gradients. *J. Aero. Sci.* **21**, 91–108.

Corrsin, S. 1958 Local isotropy in turbulent shear flow. *NACA Research Memo.* **58B11**.

Dong, Siwei, Lozano-Durán, Adrin, Sekimoto, Atsushi & Jiménez, Javier 2017 Coherent structures in statistically stationary homogeneous shear turbulence. *Journal of Fluid Mechanics* **816**, 167208.

Gungor, A.G., Maciel, Y., Simens, M.P. & Soria, J. 2016 Scaling and statistics of large-defect adverse pressure gradient turbulent boundary layers. *Int. J. Heat Fluid Flow* **59**, 109–124.

Jiménez, J. 2013 Near-wall turbulence. *Phys. Fluids* **25**, 101302.

Kitsios, V., Atkinson, C., Sillero, J. A., Borrell, G., Gungor, A. G., Jiménez, J. & Soria, J. 2016 Direct numerical simulation of a self-similar adverse pressure gradient turbulent boundary layer. *Int. J. Heat and Fluid flow* **61**, 129–136.

Kitsios, V., Atkinson, C., Sillero, J. A., Borrell, G., Jiménez, J., Gungor, A. G. & Soria, J. 2015 Direct numerical simulation of a self-similar adverse pressure gradient turbulent boundary layer. In *9th. Symp. on Turbulence and Shear Flow Phenomena (TSFP-9). The University of Melbourne, Australia, June*.

Kitsios, V., Sekimoto, A., Atkinson, C., Sillero, J.A., Borrell, G., Gungor, A. Gul, Jiménez, J. & Soria, J. 2017 Direct numerical simulation of a self-similar adverse pressure gradient turbulent boundary layer at the verge of separation. *(under review)* .

Krogstad, Per-Åge & Skåre, P. E. 1995 Influence of a strong adverse pressure gradient on the turbulent structure in a boundary layer. *Phys Fluids* **7**, 2014–2024.

Lele, S. K. 1992 Compact finite difference schemes with spectral-like resolution. *J. Comput. Phys.* **103**, 16–42.

Lighthill, M. J. 1963 *Introduction: Boundary layer theory. In Laminar Boundary Layers (L. Rosenhead, ed.)*. Oxford Univ. press.

Lozano-Durán, A., Flores, O. & Jiménez, J. 2012 The three-dimensional structure of momentum transfer in turbulent channels. *J. Fluid Mech.* **694**, 100–130.

Lozano-Durán, A. & Jiménez, J. 2014 Effect of the computational domain on direct simulations of turbulent channels up to $Re_\tau = 4200$. *Phys. Fluids* **26**, 011702.

Mellor, G. L. & Gibson, D. M. 1966 Equilibrium turbulent boundary layers. *J. Fluid Mech.* **24**, 225–253.

Schatzman, D. M. & Thomas, F. O. 2017 An experimental investigation of an unsteady adverse pressure gradient turbulent boundary layer: embedded shear layer scaling. *J. Fluid Mech.* **815**, 592642.

Sekimoto, A., Dong, S. & Jiménez, J. 2016 Direct numerical simulation of statistically stationary and homogeneous shear turbulence and its relation to other shear flows. *Phys. Fluids* **28**, 035101.

Sillero, Juan A, Jiménez, Javier & Moser, Robert D 2013 One-point statistics for turbulent wall-bounded flows at Reynolds numbers up to $\delta^+ \approx 2000$. *Phys. Fluids* **25**, 105102.

Soria, Julio & Cantwell, Brian J 1994 Topological visualisation of focal structures in free shear flows. *Appl. Sci. Res.* **53** (3-4), 375–386.

Soria, J., Kitsios, V. & Atkinson, C. 2016 On the identification of intense Reynolds stress structures in wall-bounded flows using information-limited two-dimensitonal planar data. *European Journal of Mechanics B/Fluids* **55**, 279–285.

Soria, J, Sondergaard, R, Cantwell, BJ, Chong, MS & Perry, AE 1994 A study of the fine-scale motions of incompressible time-developing mixing layers. *Phys. Fluids* **6**, 871–884.

Townsend, A. A. 1960 The development of turbulent boundary layers with negligible wall stress. *J. Fluid Mech.* **8** (01), 143–155.

Townsend, A. A. 1976 *The Structure of Turbulent Shear Flows, 2nd ed.*. Cambridge U. Press.

Wygnanski, I. & Fiedler, H. E. 1970 The two-dimensional mixing region. *J. Fluid Mech.* **41(02)**, 327–361.

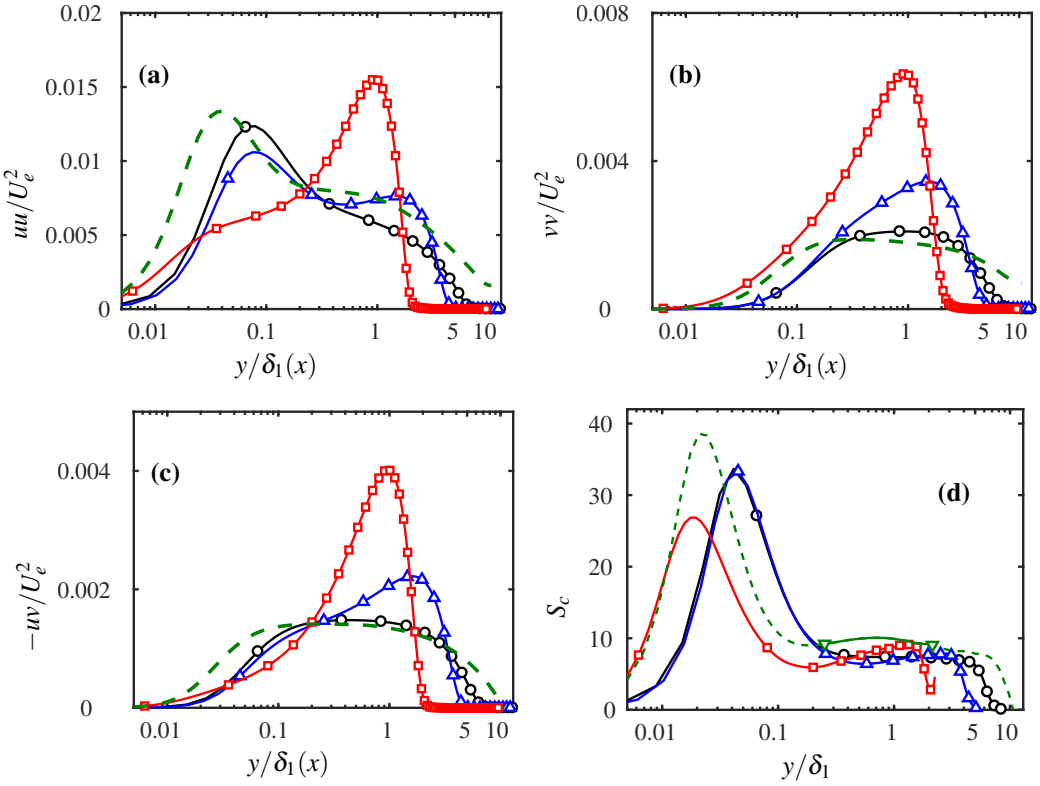

Figure 1. (a) The streamwise velocity fluctuation uu/U_e^2, (b) The vertical velocity fluctuation vv/U_e^2,(c) the Reynolds stress $-uv/U_e^2$ as a function of y/δ_1: (black) ZPG-TBL; (blue) mild APG-TBL ($\beta = 1$); (red) strong APG-TBL ($\beta = 39$); (green) channel turbulence at $Re_\tau \approx 4200$ Lozano-Durán & Jiménez (2014). Statistics are averaged in the domain of interest. (d) the Corrsin shear parameter Corrsin (1958), $S_c \equiv (\partial U/\partial y)q^2/\varepsilon$, where $q^2 \equiv u^2 + v^2 + w^2$, as a function of $y/\delta_1(x)$. The shear parameter is $S_c \approx 7$–9 both in homogeneous shear turbulence Sekimoto *et al.* (2016) and in the logarithmic layer of wall-bounded flows Jiménez (2013) (the solid line with lower triangles represents the logarithmic layer).

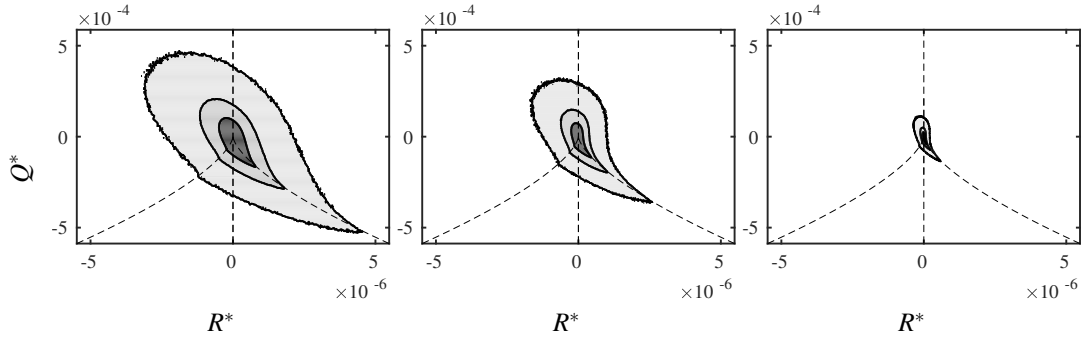

Figure 2. Joint probability density function between $Q^* = Q/(\sqrt{Re_{\delta_1}}U_e/\delta_1)^2$ and $R^* = R/(\sqrt{Re_{\delta_1}}U_e/\delta_1)^3$ for zero-pressure-gradient turbulent boundary layer flow with $Re_{\delta 1} \approx 5000$ in (left) buffer layer, $y/\delta_1 \approx 0.1$ (centre) logarithmic layer, $y/\delta_1 \approx 0.3$ (right) outer region $y/\delta_1 \approx 1.0$. The iso-probability contours are 60%, 80%, and 95% of the data. The data is averaged in the domain of interest.

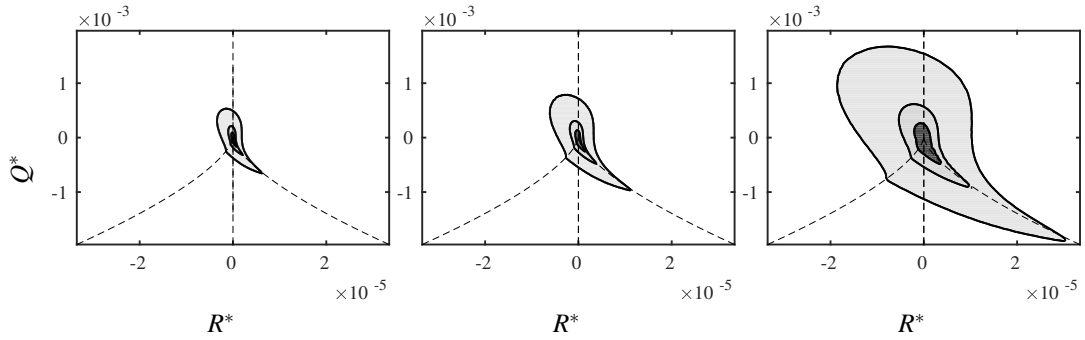

Figure 3. Joint probability density function between Q^* and R^* for self-similar adverse-pressure-gradient turbulent boundary layer ($\beta = 39$) with $Re_{\delta 1} \approx 25000$ in (left) $y/\delta_1 \approx 0.1$ (centre) $y/\delta_1 \approx 0.3$ (right) outer region, $y/\delta_1 \approx 1.0$. The data is the streamwise average in the domain of interest, assuming the self-similarity.

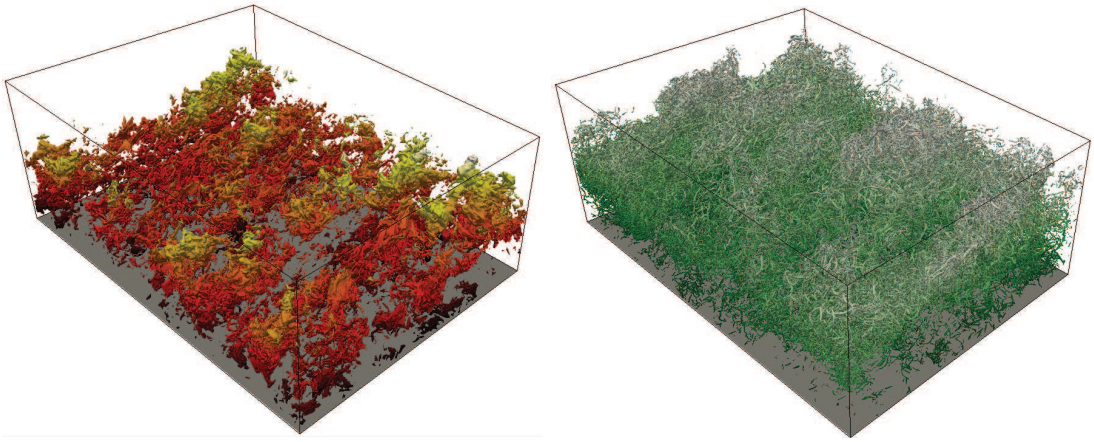

Figure 4. The region of intense Reynolds stress (left, red) and the second invariant of the velocity gradient tensor (right, green) in the self-similar APG-TBL ($\beta = 39$). Only a quarter of the domain of interest $[L_{DoI}, 0.27L_y, L_z] = [6.4, 3.43, 8.8]\delta_1(x_{\mathrm{DoI}})$ is shown, where L_{DoI}, L_y, L_z represents the streamwise, wall-normal and spanwise dimension of DoI. The threshold for the isosurfaces is $-uv/U_e^2 = 0.016$, which is 4 times larger than the outer peak of APG-TBL, and $Q^* = 10^{-3}$ (see figure 3). Note that the free-stream velocity U_e and outer length scale δ_1 is a function of the streamwise position x, and δ_1 grows 34% within the DoI. The flow is from left to top-right. The colourmap of isosurfaces is the distance from the wall, and the white colour represents $3\delta_1(x)$.

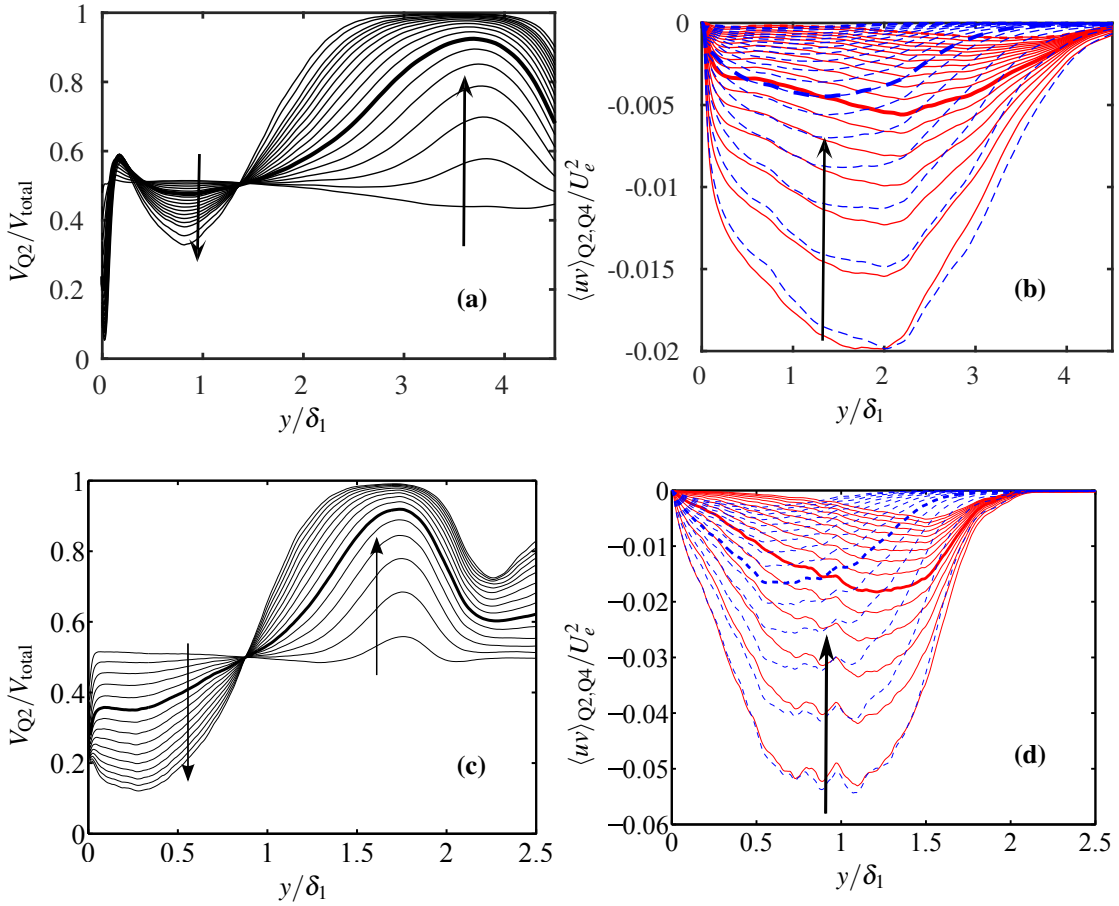

Figure 5. (a,c) The volume fraction of ejections (Q2) and sweeps (Q4), conditioned by $\tau_{xy}^* < -C_\tau u^* v^*$. The lines are $h_\tau = [0.25 : 0.25 : 4.0]$, and the thick line represents $C_\tau = 1.75$. The arrow indicates the increase of C_τ. (b,d) the Reynolds stress conditioned on the uv-structures; (red solid) Q2; (blue dashed) Q4. The lines are the same with (a). (a, b) $\beta = 1$, (c,d) $\beta = 39$.